Inorganic Chemistry

ARTICLE

pubs.acs.org/IC

Synthesis, Structure, and Bonding of Orthorhombic $R_5Au_2Te_2$ (R = Lu, Ho, Dy, Y). Electronic Structure of the Binary Parent Valence Compound Eu_5As_4

Ping Chai and John D. Corbett*

Department of Chemistry, Iowa State University, Ames, Iowa 50011, United States

Supporting Information

ABSTRACT: Four examples of $R_5Au_2Te_2$ (*vec* = 29 e^-; R = Lu, Ho, Dy, Y) have been synthesized by high-temperature solid-state techniques, isotypic examples of $Tm_5Sb_2Si_2$ (*vec* = 33 e^-) and binary Eu_5As_4 (*vec* = 30 e^-). The crystal structure was established for $Lu_5Au_2Te_2$, (orthorhombic *Cmce* (No. 64), *a* = 15.056(2), *b* = 7.749(1), *c* = 7.754(1) Å, and *Z* = 4), in which pairs of tellurium layers alternate with two-dimensional (2D) Lu_5Au_2 slabs that are aggregated in such a way that each Au_2-centered bi-trigonal prism (BTP) of Lu interconnects four other identical units, with the remaining cavities filled by nominal body-centered Lu cubes. The metal−metal aggregation in this structure provides a novel building unit in ternary rare-earth-metal-rich tellurides. Linear-muffin-tin-orbital (LMTO) electronic structure calculations and COHP analyses reveal that $Lu_5Au_2Te_2$ is a poor metal with Au_2 dimers and strong polar Lu−Au and Lu−Te interactions. The first theoretical analysis of the binary parent structure Eu_5As_4 (*vec* = 30 e^-) provides a simpler description of the equivalent orbital interactions and a closed shell gap in terms of the idealized $(Eu^{2+})_5(As_2^{4-})(As^{3-})_2$ representation, particularly for the explicit filled As_2 levels σ_s, σ_s^*, σ_p, π, π^*, plus empty σ_p^*. Crystal Orbital Hamilton Population (−COHP) data illuminate the prominent roles that polar bonding of Eu−As or Lu−Te and Lu−Au and relativistic effects with gold play in these, the former corresponding to 83% and 86% of the total Hamilton population for Eu_5As_4 and $Lu_5Au_2Te_2$, respectively.

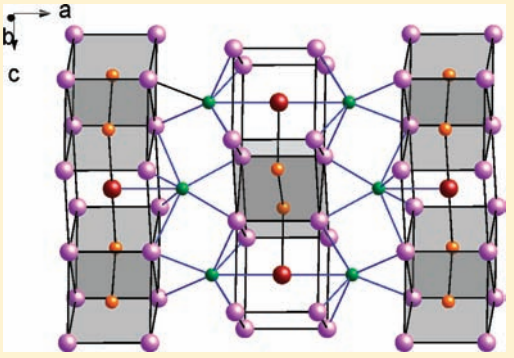

INTRODUCTION

The exploratory syntheses of new solid state compounds have played significant roles in chemistry and material science fields and have led to the discovery of thousands of compounds with diverse structures, bonding and physical properties. The investigations of metal-rich compounds have introduced a notable variety of new phases with unprecedented structures, which have not only enriched the chemistry but also provided insights into the relationships between various metal−metal bonding features.[1] The metal-rich cluster phases were initially identified among the halides of group 4, 5, and 6 metals and then in electron-poorer group 3 metals, which studies were later extended to rare-earth-metal-rich tellurides.[2,3] The additional incorporation of late transition metals into these earlier frameworks contributes to the overall stability of a diverse field of ternary phases, especially in rare-earth-metal-rich halides and tellurides.[4] Ternary tellurides display more diverse metal-rich clusters and more complex, two-dimensional (2D) or three-dimensional (3D) network structures because only half as many anions are required to yield about the same valence electron count per network metal atom (∼2) as in the halides.[5−7]

To date, three types of fundamental building units have been discovered in ternary rare-earth-metal-rich tellurides. The late transition-metal-centered tricapped trigonal prisms (TCTP) of R are the most common building unit among many different formula types: $Er_7Ni_2Te_2$,[8] $Lu_7Z_2Te_2$ (Z = Ni, Pd, Pt),[9] R_6ZTe_2 (R = Sc, Dy; Z = Mn, Fe, Co, Ni),[10,11] and $Er_{17}Ru_6Te_3$.[12] A second basic building unit is the alternating trans-face-sharing cubes and pairs of square antiprisms centered by late transition-metal in $Sc_{14}Z_3Te_8$ (Z = Os, Ru).[13] The third group, puckered rare-earth-metal six-rings centered by late transition-metals, are presented in $Sc_5Ni_2Te_2$,[14] $Y_5Z_2Te_2$ (Z = Fe, Co, Ni),[15] Gd_4NiTe_2 and $Er_5M_2Te_2$ (M = Co, Ni) compounds.[16] These fundamental building units are usually condensed into infinite one-dimensional (1D) columns, which then interconnect through different condensation modes to form 2D sheets and finally 3D structures with diverse motifs.

One interesting feature in these tellurides is that different compounds with the same formula types display more than one structure type. For example, the $Er_7Ni_2Te_2$ has an orthorhombic structure, but the $Er_7Au_2Te_2$ type shows a monoclinic structure in which the 4 × 2 zigzag condensed chains of TCTP obviously differ from the slightly puckered TCTP sheets in the former.[17] Also, the Sc_6ZTe_2 (Z = Mn, Fe, Cu, Ni) compounds are ordered ternary variants of the hexagonal Fe_2P-type structure, whereas

Received: July 13, 2011
Published: October 12, 2011

Table 1. Lattice Constants Refined from Guinier Powder Data for $R_5Au_2Te_2$ (R = Lu, Ho, Dy, Y) Phases

compound	a/Å	b/Å	c/Å	volume/Å^3	reflections for refinement
$Lu_5Au_2Te_2$	15.056(2)	7.749(1)	7.754(1)	904.7(2)	13
$Ho_5Au_2Te_2$	15.226(1)	7.8726(9)	7.8537(9)	941.4(1)	11
$Dy_5Au_2Te_2$	15.284(1)	7.8980(9)	7.8681(9)	949.8(1)	11
$Y_5Au_2Te_2$	15.307(1)	7.9179(9)	7.906(1)	958.3(1)	11

the Sc_6ZTe_2 (Z = Ag, Cu, Cd) phases crystallize as an orthorhombic Sc_2Te-type derivative.[18] The orthorhombic $Y_5Ni_2Te_2$ (*Cmcm*) and $Sc_5Ni_2Te_2$ (*Pnma*) have a common basic building unit, but they differ in metal−metal aggregations; in the former columns of rare-earth-metal six-rings interconnect via transvertices to form 2D metallic sheets, but in the latter connect side-by-side in double columns. It is obvious that the stable structure types for particular compositions depend on both R and Z as well as on atom sizes, valence electron concentrations, the ratio of host R to centered Z, and metal-to-nonmetal proportions. Of course, the interrelationships among these factors are complex and not well understood. More examples are required to provide insights into the mutual interplay of these variables and the way they influence the structural features.

Within this context we have focused on new gold-containing rare-earth-metal tellurides and bonding motifs, motivated also by earlier discoveries in this area and elsewhere[19] of novel structures and stoichiometries that arise evidently because of the special relativistic effects of gold. (The enhanced mixing of nominal 5d[10] states in bonding levels is an important manifestation of these.[17,19]) Only three examples of the combination of rare-earth-metal, gold, and tellurium are known to date, $Er_7Au_2Te_2$, $Lu_7Au_2Te_2$, and $Y_7Au_2Te_2$.[17] In the present paper, we report a new family of $R_5Au_2Te_2$ (R = Lu, Ho, Dy, Y) compounds. The configuration of $Lu_5Au_2Te_2$ breaks from the traditional 1D rare-earth-metal column structures in the tellurides and presents a novel metal−metal aggregation, which may provide a new path to explore potential tellurides. By good fortune, the structural binary parent of these compounds, Eu_5As_4, which was well determined by Wang et al. in 1978,[20] now allow a clear theoretical analysis of a more nearly ideal bonding in this lower charged example.

EXPERIMENTAL SECTION

Synthesis. All materials were handled in a He or Ar-filled glovebox. The starting materials were Lu, Ho, Dy, Tb, Y, Sc (Ames laboratory, 99.95% total), Au (Ames laboratory, 99.95%), and Te pieces (Aldrich, 99.99%). Crystals of $Lu_5Au_2Te_2$ were first obtained during an exploratory investigation of that system. To reduce Te activity in subsequent reactions, Lu_2Te_3 was first synthesized by reacting Lu and Te in 2:3 proportions in a fused silica tube that had been sealed off in a high vacuum and then heated at 450 °C for 12 h and at 900 °C for 72 h. Guinier X-ray powder diffraction data showed only the target phase. A mixture of Lu, Au, and Lu_2Te_3 with Lu:Au:Te = 5:2:2 proportions on a ∼350 mg scale was pressed into a 10 mm diameter pellet with a hydraulic press. The pellet was then arc-melted on a copper hearth in the glovebox for about 15 s at a current of 25 A, turned over, and remelted to improve homogeneity. The weight loss during arc-melting was about 1%. The button was finally sealed into a tantalum tube and annealed at 1200 °C for one week in a graphite-heated vacuum furnace (Labmaster Thermal Technology Inc. 1000−2560-FP20) at < $\sim 10^{-6}$ Torr, then allowed to cool radiatively inside the furnace. The product was crushed with the aid of an agate mortar into small crystals that were suitable for single-crystal X-ray diffraction. The powder pattern data at this point revealed what turned out to be ∼90% $Lu_5Au_2Te_2$ with small amounts of LuTe as an impurity. The compound is stable in air at room temperature for a couple of months, which was proved by X-ray powder diffraction patterns.

Similar reactions yielded the analogous products of Ho, Dy, Y with ∼60%, ∼70%, ∼75% yields, respectively, accompanied by the corresponding RTe and some unknown phases. It should be noted that the annealing temperature for these three had to be kept below 1100 °C (1080 °C was used), otherwise the samples attacked the Ta wall and the remaining collectable products were mainly HoTe, DyTe, and YTe. The reactions with Tb and Sc were unproductive, giving only some mixed binary phases.

Powder X-ray Diffraction. Powder diffraction patterns were recorded using a Huber Guinier 670 (image-plate) diffractometer with Cu Kα1 radiation (λ = 1.540598 Å). The samples were ground to a fine powder in the glovebox and evenly distributed between two Mylar films, which were then mounted between Al rings. Diffraction data were collected immediately in the 2θ range of 4−100° over 30 min. Estimated yields in vol % were achieved by comparison of the observed patterns with those calculated from the refined structure. Experimental and calculated powder patterns for $Lu_5Au_2Te_2$ are compared in Supporting Information, Figure S1. The lattice parameters listed in Table 1 for these members of the $R_5Au_2Te_2$ family were obtained by least-squares refinements of measured and indexed powder pattern lines over 2θ = 10−50 °.

Single-Crystal Diffraction Studies. Several black, irregularly shaped crystals of $Lu_5Au_2Te_2$ were mounted in glass capillaries. Crystal qualities were checked, and the best crystal was taken for a data set collection on a Bruker AXS SMART APEX CCD-based X-ray diffractometer with monochromatized Mo Kα radiation. Three sets of 606 frames with exposure times of 10 s per frame were collected at room temperature over the angular range 5.42° ≤ 2θ ≤ 52°. The intensities were integrated with SAINTPLUS,[21] and absorption corrections were applied with the package program SADABS.[21,22] A total of 3261 reflections was measured, of which 468 were unique and observed with R(int) = 4.97%. The XPREP subprogram in the SHELXTL[23] software package was used for the space group determination, for which E-value statistics and systematic absences consistently indicated *Cmce* (newer description of *Cmca*). The structure was solved by direct methods and refined by full-matrix least-squares method on F_o^2 with the aid of SHELXTL-6.10. After isotropic refinement, the final refinement with anisotropic ellipsoidal converged at R_1, wR_2 = 2.24, 5.29% ($I > 2\sigma(I)$) for the composition $Lu_5Au_2Te_2$. The difference Fourier map showed featureless residual peaks of 1.82 and −1.92 e/Å^3 that were 1.10 and 0.98 Å from gold atoms. The refined lattice parameters from powder pattern data were employed to refine the final atomic distances because of their greater accuracy. Some crystallographic and refinement data for the structure are listed in Table 2. The corresponding atomic coordinates and isotropic-equivalent displacement parameters are given in Table 3. The interatomic distances and −ICOHP data are shown in Table 4. More refinement data and anisotropic displacement parameters are provided in Supporting Information. Several more crystals were structurally characterized with the same results.

Theoretical Calculations. Tight-binding electronic structure calculations were performed for $Lu_5Au_2Te_2$ according to the linear-muffin-tin-orbital (LMTO) method in the atomic sphere approximation (ASA).[24] The radii of the Wigner−Seitz (WS) spheres were assigned automatically

dx.doi.org/10.1021/ic201492z |*Inorg. Chem.* 2011, 50, 10949–10955

Table 2. Selected Crystal and Refinement Data for $Lu_5Au_2Te_2$

empirical formula	$Lu_5Au_2Te_2$
crystal system	orthorhombic
space group, Z	*Cmce* (No. 64), 4
a (Å)	15.056(2)
b (Å)	7.749(1)
c (Å)	7.754(1)
volume (Å^3)	904.7(2)
d_{calc} (g/cm^3)	11.189
μ (mm^{-1})	92.55
index ranges	$-18 \le h \le 18$, $-10 \le k \le 9$, $-9 \le l \le 9$
reflections collected	3261
independent, obs. reflections	468 (R_{int}= 0.0497)
data/parameters	468/25
goodness-of-fit on F^2	1.08
R indices [$I > 2\sigma(I)$]	R_1 = 0.0224, wR_2 = 0.0529
R indices (all data)	R_1 = 0.0248, wR_2 = 0.0540
largest diff. peak, hole (e/Å^{-3})	1.82 [1.10 Å from Au], −1.92 [0.98 Å from Au]

Table 3. Atomic Coordinates and Equivalent Isotropic Displacement Parameters (Å^2 × 10^4) for $Lu_5Au_2Te_2$

atom	Wyckoff	symmetry	x	y	z	U_{eq}[a]
Te	8*d*	2	0.2084(1)	0	0	80(3)
Au	8*f*	*m*	0	0.1360(1)	0.3656(1)	70(2)
Lu1	4*a*	2/*m*	0	0	0	79(3)
Lu2	16*g*	1	0.1224(1)	0.3378(1)	0.1610(1)	89(2)

[a] U_{eq} is defined as one-third of the trace of the orthogonalized U_{ij} tensor.

Table 4. Interatomic Distances (Å) and −ICOHP Values [eV/bond·mol] in $Lu_5Au_2Te_2$[a]

bond	n	distance	−ICOHP	bond	n	distance	−ICOHP
Au−Lu2	16	2.8912(7)	1.37	Lu2−Lu1	16	3.4357(6)	0.37
Au−Lu2	16	2.9464(7)	1.15	Lu2−Lu1	16	3.4480(6)	0.38
Au−Lu2	16	2.9629(8)	1.11	Lu2−Lu2	8	3.542(1)	0.15
Au−Lu1	8	3.0069(7)	1.29	Lu2−Lu2	8	3.685(1)	0.24
Au−Lu1	8	3.0249(7)	1.26	Te−Lu2	16	3.103(1)	0.81
Au−Au	4	2.964(1)	1.06	Te−Lu2	16	3.1756(7)	0.75
Te−Lu1	8	3.137(1)	0.90	Te−Lu2	16	3.1889(7)	0.74

[a] n is the number of interactions of each type per unit cell.

so that the overlapping potentials would be the best possible approximations to the full potentials.[25] For space filling within ASA, 12 empty spheres (ES) were introduced within the limit of 18% overlap between any atom-centered spheres. The WS radii were Lu, 3.32−3.50 Å; Au, 3.01 Å; Te, 3.38 Å; ES, 1.86−2.04 Å. The calculations used a basis set of Lu-6s/(6p)/5d, Au-6s/6p/5d, Te-5s/5p/(5d) (downfolded[26,27] orbitals in parentheses) with Lu 4f[14] treated as core, and the reciprocal space integrations were performed on grids with 365 irreducible k points. Exchange and correlation were treated in a local density approximation, and scalar relativistic effects were included. For bonding analysis, the energy contributions of filled electronic states for all Lu−Lu, Lu−Au, Lu−Te, and Au−Au contacts were calculated as functions of the energy

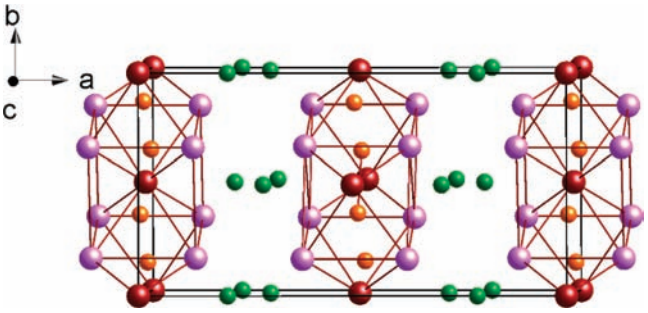

Figure 1. ~[001] view of the orthorhombic $Lu_5Au_2Te_2$ structure (*Cmce*). The atoms are marked as follows: Au, orange; Lu1, dark red; Lu2, lavender; Te, green.

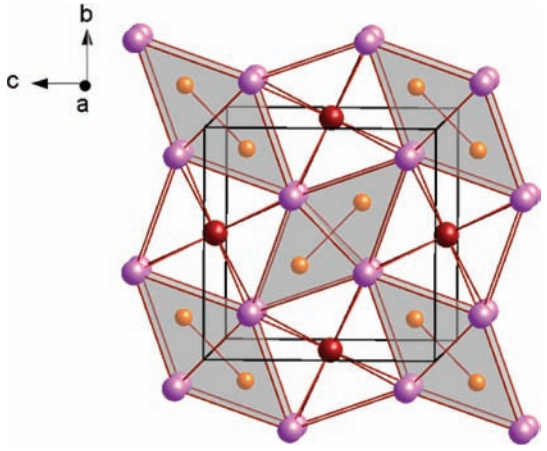

Figure 2. ~[100] view of part of a single Lu_5Au_2 2D slab. Two planes define condensed BTP with Lu1 and Au_2 dimer in a mirror plane between them. Au, orange; Lu1, dark red; Lu2, lavender.

according to the crystal orbital Hamilton population (COHP) method.[28] Weighted integration of COHP data for each bond type over all filled states yielded ICOHP, the Hamilton overlap populations. For comparison, a like calculation was also performed for the isostructural parent Eu_5As_4.[20] The WS radii were Eu, 3.54−3.67 Å; As, 2.75−3.14 Å; ES, 1.46−1.94 Å. The basis set included Eu-6s/(6p)/5d (4f^7 as core) and As-4s/4p/(4d). A calculation according to the local spin density approximation showed no significant problems were introduced by the 4f^7 states on Eu.

RESULTS AND DISCUSSION

Structural Description of $Lu_5Au_2Te_2$. The compound crystallizes in the $Tm_5Sb_2Si_2$ structure type in space group *Cmce*, an ordered variant of *Pnma* Eu_5As_4. A ~[001] section of this structure is given in Figure 1, in which infinite 2D Lu_5Au_2 slabs stack alternately with pairs of tellurium layers along the horizontal a axis. Each slab contains a mirror plane (a = 0, $^1/_2$, 1) and adjoining slabs are related by b glides at a = $^1/_4$, $^3/_4$. Figure 2 is a cross section of a single 2D slab along a for somewhat more than one unit cell. The motif contains two kinds of condensed building units: bi-trigonal prisms (BTP) and pseudocubes of Lu2 centered by Lu1. The former consists of two Au-centered trigonal prisms that share a rectangular face along a and an inversion point at ($^1/_2$, 0, 0), and so forth. This leads to the formation of tilted Au dimers in (200) mirror planes that are 2.964(1) Å long, a strong interaction according to the calculation

dx.doi.org/10.1021/ic201492z |*Inorg. Chem.* 2011, 50, 10949–10955

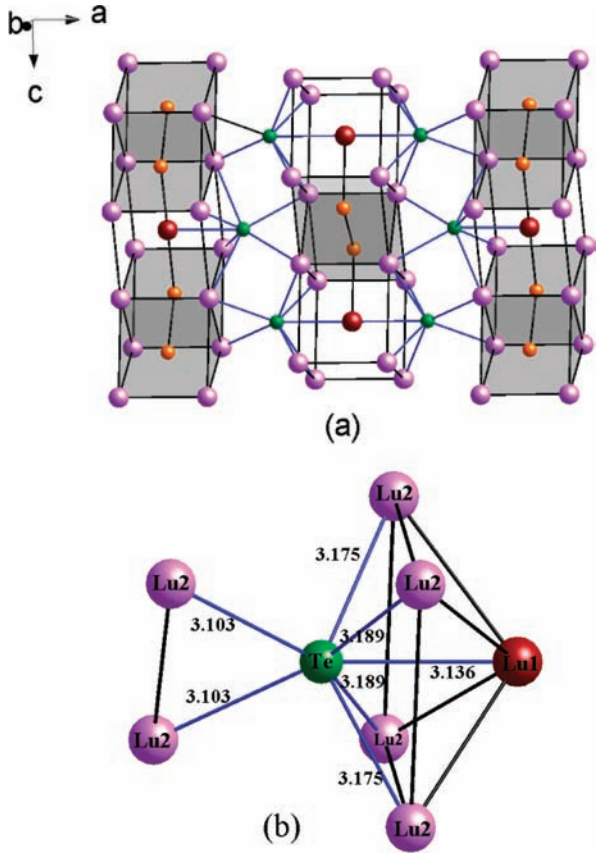

Figure 3. (a) ~[010] projection in which all Te atoms are in one *ac* plane for $Lu_5Au_2Te_2$. (b) The bonding environment of Te atom with marked distances between Te and Lu. Au, orange; Lu1, dark red; Lu2, lavender; Te, green.

below. This is the first example of late-transition metal dimers within BTP in any ternary rare-earth-metal-rich cluster compound. The Lu2−Lu2 bonds in the shared rectangular face of the BTP are 3.685(1) Å along *a* and 3.543(1) Å within the *bc* plane, distances that are in accord with those found among other Lu compounds.[7] The 2D slab is generated in such a way that each BTP interconnects four such units via shared Lu2−Lu2 edges (3.685(1) Å) with the remaining cavities filled by the Lu1 atoms that lie on inversion centers and center Lu2 pseudocubes. Each Au atom has six close Lu2 neighbors in the trigonal prism, from 2.8912(7) Å to 2.9629(8) Å, and two coplanar Lu1 neighbors 3.0069(7) Å and 3.0249(7) Å; the latter are somewhat more important energetically (below). The Lu1 atom is bonded to eight Lu2 at 3.4356(6) Å (4×) and 3.4481(6) Å (4×), 0.10 to 0.24 Å less than the Lu2−Lu2 contacts.

The parallel Lu_5Au_2 slabs order along *a* with *b*/2 displacements and are separated by intervening zigzag chains of Te in two layers. The Lu2−Lu2 distances between two adjacent slabs are 4.0833(8) Å, illuminating the negligible direct interactions between them. Figure 3a is a projection of three slabs along *b* in which all Te atoms lie in one plane, and Figure 3b emphasizes the Te bonding environment and the remarkable role of Te atoms in interbridging the slabs. Each Te atom bonds to four Lu2 plus one Lu1, all in a pseudocube on one side of the slab (Figure 3b), and to the shared Lu2−Lu2 edge of a BTP on the other side that has a *b*/2 displacement. The Te atoms thus form zigzag chains along *c* with repeats of *b*/2 (Figure 1) to hold a pair of slabs together. The closest Te−Te and Au−Te are 4.0723(7) Å and 4.346(1) Å, reflecting the absence of significant bonding between the electronegativity atoms, as expected and found in many systems.[14,15,17]

Theoretical Calculations. The total DOS, atomic and orbital partial DOS (pDOS), and the −COHP data for different pairwise interactions in $Lu_5Au_2Te_2$ are plotted in Figure 4a−e. The Fermi level (E_F) cuts the edge of the upper valence band in the total DOS at which the main contributions are from Lu 5d and Au 6p, demonstrating a metallic character. $Lu_5Au_2Te_2$ has a valence electron count of 29 e^- ($5 \times 3 + 2 \times 1 + 2 \times 6 = 29$), one electron short of a deep pseudogap at 30 e^-, and this is followed by a second moderate pseudogap at 32 e^-. These features should be associated with the components of the crystal structure and their bonding. At this point a search of Pearson number file for this structure (*oS*36) quickly took us to the binary parent compound Eu_5As_4 (30 e^-), the structure of which was published in 1978,[20] and to a few others: Ba_5Sb_4 (30 e^-) in one of the two reported structures types, a difference that has not been resolved,[29,30] and to a $R_5Sb_2X_2$ family (R = Y, Tb, Dy, Ho, Er, Tm; *X* = Si or Ge, 33e^-).[31] However, none of these has been described in terms of the bonding, although inspection of atom distribution in the parent component quickly suggests the extreme valence representation $(Eu^{2+})_5(As_2^{4-})(As^{3-})_2$ could pertain.

To better understand the theoretical results for the new ternary phase, a like calculation was carried out for the evidently simpler Eu_5As_4, and the two essential results, the DOS and −COHP data, are shown in Figure 5 (the pDOS data are in Supporting Information). The notable contrast in band resolution and other details between $Lu_5Au_2Te_2$ and Eu_5As_4 (Figures 4 versus 5) certainly must originate at least in part because of the presence of trivalent Lu versus divalent Eu in the two, the greater polarizing effects of the former in broadening bands and distorting structures being well-known. Another appreciable difference occurs between the dimer components Au_2 and As_2, the latter being considerably more familiar (the structure of Eu_2As_2 is also known.[32]). The clearer results from the Eu_5As_4 calculations will be analyzed first. The total DOS for Eu_5As_4, Figure 5a, displays two distinct gaps that roughly correspond to the two in $Lu_5Au_2Te_2$. The Fermi level cuts the first gap at 0 eV (30 e^-), indicating a probable semiconduction property for Eu_5As_4. Classically, the formal charges on the As_2 dimers and As monomers are −4 and −3, respectively, for closed shell configurations of As.[33] Therefore, Eu_5As_4 can be idealized in term of individual components as $(Eu^{2+})_5(As_2^{4-})(As^{3-})_2$, with a 30 valence electrons band leading to the principal valence gap in DOS.

The DOS and −COHP functions are sufficient to allow a fairly clear and easy analysis of the bonding in the rest of Eu_5As_4. The pDOS for Eu1, Eu2, As1, and As2 (vice Au) are shown in Figure 5a and the corresponding −COHP data in Figure 5b. The more explicit DOS and −COHP data for the As1 monomer and the $(As2)_2$ dimer are shown in orange and green in each case. Starting at the higher binding energies, the As2 4s states lie in two very sharp peaks around −12 and −10 eV, which correspond to the σ_s and σ_s^* bands, as demonstrated by the −COHP data. The critical As2 4p states fall just above −5 eV and generate four characteristic and distinctive bands: σ_p around −4 eV, π between −3.8 and −3.0 eV, π^* from there to ~−0.5 eV, and σ_p^* just above E_F. The −COHP data verify the assignments with respect to the individual bonding/antibonding characteristics. Electronic

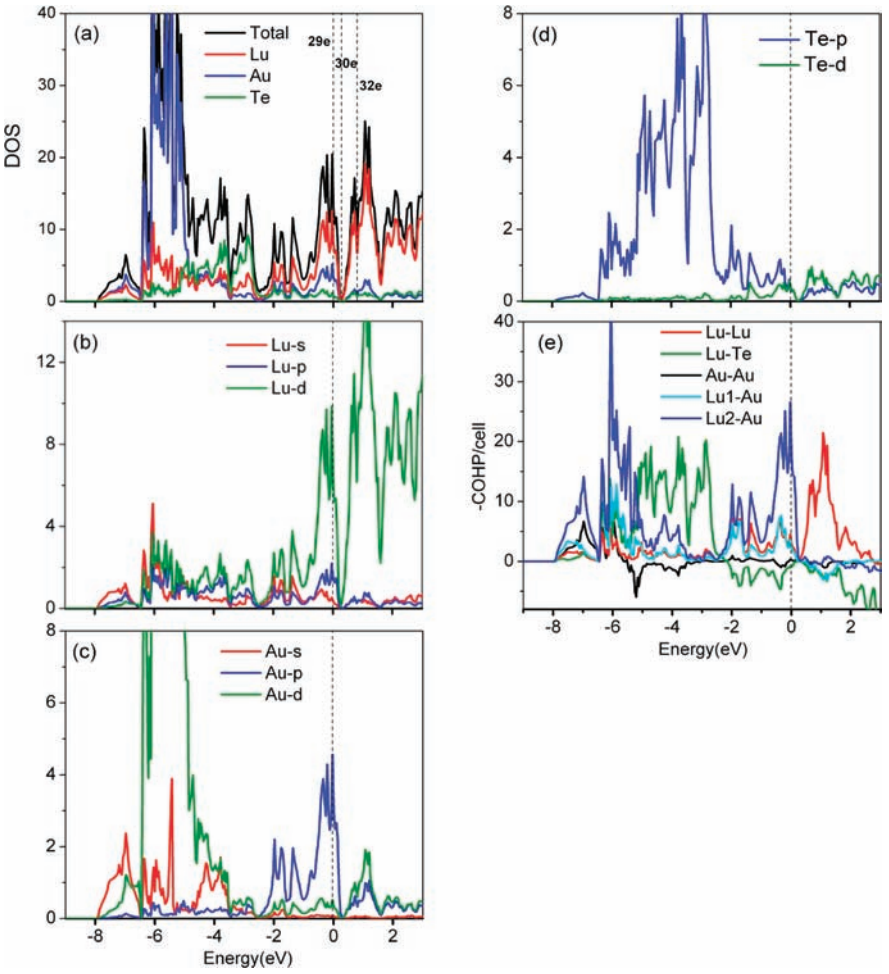

Figure 4. (a) Total densities of states (DOS) and partial DOS by atom for $Lu_5Au_2Te_2$ (29e). (b−d) Partial DOS by orbital type for each element. (e) Crystal orbital Hamilton populations (−COHP, eV/cell). The dashed lines mark the Fermi energy (E_F) at 29e and two pseudogaps at 30e and 32e.

states on the monomeric As1 atoms, which combine with Eu1 and Eu2 in interslab bonding (Figure 3), are confined to 4p functions within −4 to 0 eV (orange) plus a sharp 4s peak around −10 eV. The 6s and 6p states for Eu1 and Eu2 disperse mostly within −4 eV to E_F, whereas their 5d states largely fall above E_F. The inter-Eu interactions that define the biprismatic and cubic components of the cation structure (Figure 2) are reflected in relatively small −COHP values (dark and light blue lines, Figure 5b) compared with the size of the polar Eu−As terms. The last are marked with black and red lines and, especially, by the large area outlined in orange in Figure 5b, corresponding to the interslab Eu−As1 bonding described for Lu−Te bonding in $Lu_5Au_2Te_2$ in Figure 3.

The sizable bands just above E_F originate from As2 4p and Eu1/Eu2 5d orbitals and correspond in part to the As2−As2 σ_p^* bond decomposition (in frozen terms) which is offset by gains in Eu1−As2, Eu2−As2, and Eu1−Eu2 bonding according to the −COHP data. This suggests a mutual correlation among the bonding environments of the As2 dimer and the neighboring Eu atoms, the σ_p^* bond breakage in As_2 shifting charge outwardly toward the nearby Eu1/Eu2 network to enhance the probably somewhat delocalized bonding therein (See inset in Figure 5b for the proportions). This description is still artificial in that the structure is unstable much above E_F, and the second pseudogap must be imaginary with these insights.

Eu_5As_4 is structurally and electronically similar to the so-called R_5Tt_4 Zintl systems (R = rare earth metal; Tt = Si, Ge). According to the proportions of dimerized interslab Tt1 atoms, three types of R_5Tt_4 compounds can be distinguished: Gd_5Si_4-type (*Pnma*, all Tt1−Tt1 dimers), $Gd_5Si_2Ge_2$-type ($P112_1/a$, half Tt1−Tt1 dimers), and Sm_5Ge_4-type (*Pnma*, no Tt1−Tt1 dimers).[34] None of these is electron-precise, and some structures are influenced by strong magnetic coupling. Eu_5As_4 is somewhat similar to Sm_5Ge_4 as neither has an interslab dimer, though the latter adopts a subgroup of the former *Cmce* and features cations with different oxidation states. However, some special electronic features can be found in Eu_5As_4: (i) the σ_s band of As2 dimers are lowest in energy compared with those reported in all the R_5Tt_4-type compounds (including their ternary derivatives achieved by doping with Ga, P, Y),[34−37] which is probably caused by the greater electronegativity of As; (ii) Eu_5As_4 is the unique example that exhibits a closed shell and thus probable semiconductor character, whereas the R_5Tt_4-type phases are either electron-rich or electron-short and thereby all of them display metallic properties; (iii) all of the bonding are optimized at E_F in Eu_5As_4, whereas the R_5Tt_4-type phases at E_F always have some contributions from σ_p^* (electron-rich phases) or π^* (electron-poorer phases) states within the intraslab Tt2 dimers. The lower field of Eu^{2+} must be important.

dx.doi.org/10.1021/ic201492z |*Inorg. Chem.* 2011, 50, 10949–10955

Note that Köhler and Whangbo[38] have also studied the electronic structure of Au_2 dimers in Ca_5Au_4, in which two nonequivalent Au_2 dimers in 12-fold environments are similar to the present Au_2 dimers in $Lu_5Au_2Te_2$, but their bonding analysis indicates a less reduced state for the Au_2 dimer, in accord with the proportion of Ca. The Au 6p states are only partially filled, leading to the approximation $(Au_2)^{4-}$. The two nonequivalent Au dimers do not allow a clear resolution of their individual electronic states, either.

The total and partial (orbital) DOS data for $Lu_5Au_2Te_2$, Figure 4, provide more details about its less ideal electronic structure. Many of the changes and complication arise from the contributions of (a) major 5d orbitals in Au_2 dimers, (b) the much more electronegative Te and Au in place of As, and (c) the increase in oxidation states of the cations from +2 to +3 and some decrease in size as well. All of the bands broaden in consequence. As shown in Figure 4b, the orbital pDOS of Lu shows mixed contributions of 5d, 6s, and 6p states from nearly −8 eV to E_F, above which the distribution is predominately 5d. The Au 5d states (Figure 4a) are involved mainly between −8 and −3 eV with some sharp 6s states mixed in over the lower range. The largest number of Au 5d states, mainly nonbonding, are confined between −6.5 and −4 eV. An unusual feature seems to be the occupied Au 6p states which occur mainly between −2.5 and +0.2 eV; that is, up to a *vec* of 30 e^-. These reflect the topping up of all Au valence orbitals and the substantial reduction of Au; the same condition applies to basically filled Te 5p states, and both lead to the substantial oxidation of Lu as reflected in the high fraction of the least penetrating Lu 5d states that lie above Fermi. These are common characteristics of many other related metal-rich compounds.[3,17,39] (On the other hand, the conclusions are in opposition to a common misinterpretation of stick drawings like Figures 2 and 3: that the many Lu−Lu connections reflect major bonding in the compound, not just geometric tie-lines.[40])

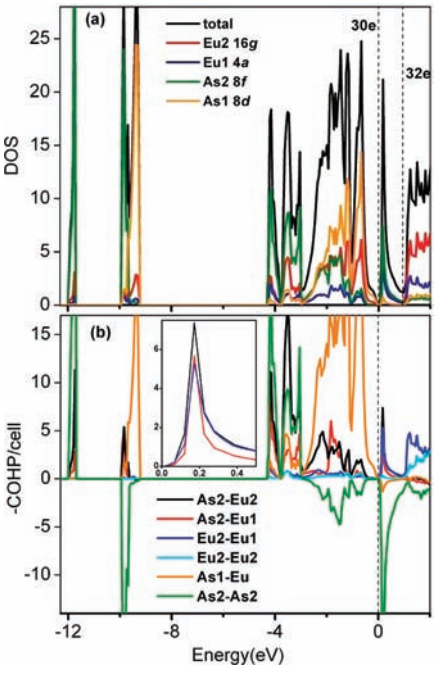

Figure 5. (a) Total densities of states (DOS) and partial DOS by atom for Eu_5As_4. (b) −COHP curves for different pairwise bond types. The inset shows a section of enlarged curves. The dashed lines mark Fermi energy (E_F) at 30e and the pseudogap at 32e.

Some features in the −COHP results can be associated with specific bonding interactions. The rather bimodal Lu−Au −COHP in Figure 4e divides into those for lower-lying Au 6s/5d states and higher Au 6p for both Lu1 and Lu2 (4:16 proportions), light and dark blue curves, respectively. The higher lying features are clearly associated with Au 6p, Figure 4c. On the other hand, the low lying states appear to be irregular and associated with several bonding patterns. However, qualitative considerations led us to notice that several −COHP patterns appeared to parallel the rather spiky Au 6s DOS distributions. The Supporting Information, Figure S3, shows that the Au 6s pDOS (red line) follows just the Au 6s contributions to the −COHP results for Au−Au, Lu1−Au, and Lu2−Au, (black, light, and dark blue lines, respectively) the same scheme as in Figure 4e except that the scales are better leveled here on a per bond·mol basis. The Lu 5d−Te 5p −COHP distribution in Figure 4e is similarly spread over ∼ −2.5 to −5 eV, the nominally filled Te 5p states not being as low-lying/electronegative. In this case the Lu1 and Lu2 contribute to the result separately. Additional antibonding Lu−Te states, probably electron pair repulsions with Te, next appear from −2 eV to above E_F but primarily only for the centered Lu1. The Lu−Lu COHP arises predominately from 5d−5d interactions, as clearly suggested by the orbital pDOS of Lu itself. All the bands are optimized at 29 or 30 e^-, reflecting the high (relative) electronic stability of $Lu_5Au_2Te_2$, except that the Lu−Au band remains weakly bonding. In terms of Hamilton bond populations, the substantial polar Lu−Au and Lu−Te interactions in $Lu_5Au_2Te_2$ are more or less frequent and important characteristics, and in other related metal-rich compounds too.[17,39] This different chemistry clearly removes the gold tellurides from a close relationship with Sm_5Ge_4-type phases, and the unlikelihood of Te_2 species, from any comparison with Gd_5Si_4, and so on.

The energy-weighted integrals of COHP data (i.e., −ICOHP) also give us some measure of relative bond population or indexes. The average −ICOHP for each bond type and the corresponding sum per cell are summarized in Table 5 for $Lu_5Au_2Te_2$ and Eu_5As_4. The parallel Lu−Lu and Eu−Eu bonding provide the smallest contributions to the total −ICOHP per bond for both compounds, and Eu^{II} is also particularly inferior in polar bonding to As2 versus Lu^{III} to Au, in which relativistic effects are also

Table 5. Average −ICOHP for Each Bond Type and the Sum Per Unit Cell in $Lu_5Au_2Te_2$ and Eu_5As_4

	$Lu_5Au_2Te_2$				Eu_5As_4			
atom pair	Lu−Lu	Lu−Au	Lu−Te	Au−Au	Eu−Eu	Eu−As1	Eu−As2	As2−As2
−ICOHP (avg., eV/bond·mol)	0.32	1.23	0.79	1.06	0.06	0.72	0.39	2.49
no. of bonds per unit cell (Z = 4)	48	64	56	4	48	56	64	4
−ICOHP (cumulative, eV/cell)	15.4	78.7	44.2	4.2	2.9	40.3	25.0	10.0
% contribution	11	55	31	3	4	51	32	13

dx.doi.org/10.1021/ic201492z |*Inorg. Chem.* 2011, 50, 10949–10955

important. The stabilities of such relative to the decomposed products are very different issues. The polar populations in each make the greater contribution, 86% in $Lu_5Au_2Te_2$ and 83% in Eu_5As_4, in parallel with the behaviors in recently reported $Er_7Au_2Te_2$.[17]

CONCLUSIONS

Synthetic reactions aiming at gold incorporation into rare-earth-metal-rich tellurides yield $Lu_5Au_2Te_2$ plus the analogues with Ho, Dy, and Y. The present $Lu_5Au_2Te_2$ (*Cmce*) exhibits the same structure type as the long known Eu_5As_4 in which the As atoms occupy both dimer and monomer positions, but with a novel way of metal−metal aggregation compared with the previously reported ternary rare-earth-metal rich tellurides. $Lu_5Au_2Te_2$ is predicted to have a metallic property because it contains only 29 e^- compared with a closed shell count of 30 e^-. The more nearly ideal Eu_5As_4 displays clear orbital components of the As_2 dimer and a good structural correlation with the calculated electronic structure. The polar bonding play significant roles in both compounds; the Lu−Au bonding makes prominent contributions of the total because of the relativistic effects of Au.

ASSOCIATED CONTENT

Supporting Information. Detailed crystallographic data in CIF form, a table of anisotropic displacement parameters for $Lu_5Au_2Te_2$, the experimental and calculated powder pattern diagram for $Lu_5Au_2Te_2$, partial DOS curves for Eu_5As_4, and a correlation of Au−s contribution with bonding states at low energy. This material is available free of charge via the Internet at http://pubs.acs.org.

AUTHOR INFORMATION

Corresponding Author
*E-mail: jcorbett@iastate.edu.

ACKNOWLEDGMENT

This research was supported by the U.S. National Science Foundation, Solid State Chemistry, via Grant DMR-0853732. All of the work was performed in the facilities of the Ames laboratory, U.S. Department of Energy.

REFERENCES

(1) Whangbo, M. H.; Canadell, E.; Foury, P.; Pouget, J. P. *Science* **1991**, *252*, 96.
(2) Corbett, J. D. *J. Alloys Compd.* **1995**, *229*, 10.
(3) Corbett, J. D. *Inorg. Chem.* **2010**, *49*, 13.
(4) Corbett, J. D. *J. Alloys Compd.* **2006**, *418*, 1.
(5) Corbett, J. D. *Inorg. Chem.* **2000**, *39*, 5178.
(6) Maggard, P. A.; Corbett, J. D. *J. Am. Chem. Soc.* **2000**, *122*, 838.
(7) Chen, L.; Xia, S. Q.; Corbett, J. D. *Inorg. Chem.* **2005**, *44*, 3057.
(8) Meng, F. Q.; Hughbanks, T. *Inorg. Chem.* **2001**, *40*, 2482.
(9) Chen, L.; Corbett, J. D. *Inorg. Chem.* **2004**, *43*, 3371.
(10) Maggard, P. A.; Corbett, J. D. *Inorg. Chem.* **2000**, *39*, 4143.
(11) Bestaoui, N.; Herle, P. S.; Corbett, J. D. *J. Solid State Chem.* **2000**, *155*, 9.
(12) Mehta, A.; Corbett, J. D. *J. Solid State Chem.* **2008**, *181*, 871.
(13) Chen, L.; Corbett, J. D. *J. Am. Chem. Soc.* **2003**, *125*, 1170.
(14) Maggard, P. A.; Corbett, J. D. *Inorg. Chem.* **1999**, *38*, 1945.
(15) Maggard, P. A.; Corbett, J. D. *Inorg. Chem.* **2004**, *43*, 2556.
(16) Magliocchi, C.; Meng, F. Q.; Hughbanks, T. *J. Solid State Chem.* **2004**, *177*, 3896.
(17) Gupta, S.; Corbett, J. D. *Dalton Trans.* **2010**, *39*, 6074.
(18) Chen, L.; Corbett, J. D. *Inorg. Chem.* **2002**, *41*, 2146.
(19) (a) Lin, Q.; Corbett, J. D. *Inorg. Chem.* **2007**, *129*, 2187. (b) Lin, Q.; Corbett, J. D. *Inorg. Chem.* **2010**, *49*, 10436.
(20) Wang, Y.; Calvert, L. D.; Gabe, E. J.; Taylor, J. B. *Acta Crystallogr.* **1978**, *B34*, 1962.
(21) *SMART*; Bruker AXS, Inc.: Madison, WI, 1996.
(22) Blessing, R. H. *Acta Crystallogr.* **1995**, *A51*, 33.
(23) *SHELXTL*; Bruker AXS, Inc.: Madison, WI, 2000.
(24) Tank, R.; Jepsen, O.; Burkhardt, A.; Andersen, O. K. *TB-LMTO-ASA Program*, version 4.7; Max-Planck-Institut fur Festkörperforschung: Stuttgart, Germany, 1994.
(25) Jepsen, O.; Aaronson, O. K. *Z. Phys. B* **1995**, *97*, 35.
(26) Lambrecht, W. R. L.; Andersen, O. K. *Phys. Rev. B* **1986**, *34*, 2439.
(27) Löwdin, P.-O. *J. Chem. Phys.* **1951**, *19*, 1396.
(28) Dronskowski, R.; Blochl, P. E. *J. Phys. Chem.* **1993**, *97*, 8617.
(29) Derrien, G.; Monconduit, L.; Tillard, M.; Belin, C. *Acta Crystallogr., Sect. C* **1999**, *55*, 1044.
(30) Brechtel, E.; Cordier, G.; Schaefer, H.; Belin, C. *Z. Naturforsch., B: Chem. Sci.* **1981**, *36*, 1341.
(31) Kozlov, A.Yu.; Pavlyuk, V. V.; Davydov, V. M. *Intermetallics* **2004**, *12*, 151.
(32) Wang, Y.; Gabe, E. J.; Valvert, L. D.; Taylor, J. C. *Acta Crystallogr.* **1977**, *B33*, 131.
(33) Miller, G. J.; Lee, C.-S.; Choe, W. *Highlights in Inorganic Chemistry*; Meyer, G., Naumann, D., Wesemann, L., Eds.; Wiley-VCH: Weinheim, Germany, 2002; p 21.
(34) Mozharivskyj, Y.; Choe, W.; Pecharsky, A. O.; Miller, G. J. *J. Am. Chem. Soc.* **2003**, *125*, 15183.
(35) Seo, D. K.; Wu, L. M.; Kim, S. H. *J. Am. Chem. Soc.* **2005**, *127*, 15682.
(36) Svitlyk, V.; Miller, G. J.; Mozharivskyj, Y. *J. Am. Chem. Soc.* **2009**, *131*, 2367.
(37) Misra, S.; Miller, G. J. *J. Am. Chem. Soc.* **2008**, *130*, 13900.
(38) Köhler, J.; Whangbo., M. *Chem. Mater.* **2008**, *20*, 2751.
(39) Gupta, S.; Maggard, P. A.; Corbett, J. D. *Eur. J. Inorg. Chem.* **2010**, *2010*, 2620.
(40) Gupta, S.; Meyer, G.; Corbett, J. D. *Inorg. Chem.* **2010**, *49*, 9949.